STRUCTURE AND PARAMETERS DEPENDENCES OF ALFVÈN WAVE CURRENT DRIVE GENERATED IN THE LOW-FIELD SIDE OF SIMULATED SPHERICAL TOKAMAKS

S.CUPERMAN, C.BRUMA, K.K OMOSHVILI
School of Physics and Astronomy,
Tel Aviv University, Israel

Abstract

Theoretical results on the wave-plasma interactions in simulated toroidal configurations are presented. The study covers the cases of large to low aspect ratio tokamaks, in the pre-heated stage. Fast waves emitted from an external antenna with different wave numbers and frequencies are considered. The non-inductive Alfvèn wave current drive is evaluated and discussed.

1. INTRODUCTION

In view of the crucial importance of the non-inductive current drive in low aspect ratio (spherical) tokamaks (LART's) [1]–[4], we have investigated the propagation and absorption-conversion of fast waves as well as generation of Alfvèn wave current drive (AW CD) in such devices [5]-[14].

In this model, fast waves launched by an external antenna penetrate a "simulated" current carrying equilibrium tokamak plasma and are partially converted into Alfven waves; these, in turn, are absorbed by plasma electrons and generate a non-inductive current drive; the simulated toroidicity and shear are arbitrarily large. Thus, this model represents a reasonable, first order description of the AW CD generated in the low field side of tokamaks, including LART's.

The solution of the problem includes: (a) the derivation in local B magnetic coordinates, of closed analytical expressions for the elements of the dielectric tensor, within the framework of resistive, two-fluid model equations; they hold well in the pre-ignated stage; (b) the derivation of analytical expressions for the field components in the region between the plasma and the metalic wall, within which the antenna is located; (c) solution of the full wave equation ($E_{||} \neq 0$) for the radio frequency (rf) field components; and (d) evaluation of the rf current drive, comprising its momentum transfer, plasma flow and dynamo components.

2. RESULTS AND CONCLUSIONS

We investigated the inverse aspect ratio dependence ($\epsilon \equiv a/R$) of the propagation, absorption and conversion as well as the AW CD in the range $01 \leq \epsilon \leq 0.9$, and for various plasma and antenna parameters. Illustrative results are presented in Figs.1-5 as follows: (i) test of the computational algorithm (Fig.1); (ii) **frequency and temperature dependence of the total power absorption, P, and total AW CD I**, for some eight ϵ-values and fixed wavenumbers (Figs.2–3); (iii) **dependence of the efficiency**, $\eta \equiv I/P$, on ϵ, temperature T and several combinations of poloidal (m) and 'toroidal' (n) wave numbers (Fig.4); and (iv) **dependence of the radial distance** (from the magnetic axis) of the conversion point, x_s, on ϵ, T, m and n (Fig.5).

The results of our study support the following conclusions. (a). The three AW CD components (i.e., dynamo, helicity injection and plasma flow) are generated in the entire range of relevant aspect ratio values; (b). for the physical parameters considered in this work, the helicity injection CD component dominates - the other (smaller) components are comparable; (c). in the case of low (large) aspect ratio configurations, the maximum efficiency of AW CD increases (decreases) with increasing poloidal wave number, $|m|$ ($m = -|m|$), and with decreasing toroidal

wave number, $|n|$ ($n = -|n|$). (d). The radial distance of the conversion layer is determined by the lower edge frequency, $\omega_L(\epsilon, T, m, n)$. Its value decreases with increasing aspect ratio and toroidal wave number as well as with decreasing poloidal wave number.

A more detailed discussion of the analytical and numerical methods used in this work as well as of the results obtained will be presented elsewhere.

References

[1] Peng, Y.K.M. and Strickler, D., Nucl. Fusion **26** (1986) 769.
[2] Intrator, T., et al., Phys. of Plasmas, **2** (1995) 2263.
[3] Morris, W., 1996 (Ed.), Proceedings of International Workshop on Spherical Torus and US - Japan Workshop for Low Aspect Ratio Tokamaks, 4-6 Dec. 1996, Culham, UKAEA.
[4] Sykes, A., et al., "Tight Aspect Ratio Tokamak Experiments and Prospects for the Future" (AIP Conf. Proc. 345) AIP Press, New York (1995) 110.
[5] Fisch, N., Rev. Mod. Phys. **59** (1987) 175.
[6] Chan, V.S., Miller, V.L., Ohkawa T., Phys. Fluids **B2** (1990) 994.
[7] Elfimov, A.G., Petržilka, V. and Tataronis, J.A., Phys. of Plasmas **1** (1994) 2882.
[8] Hasegawa, A., Chen, L., Phys. Lett. **32** (1974) 454.
[9] Litwin, C., Phys. of Plasmas **1** (1994) 515.
[10] Ono, M., Phys. of Plasmas **2** (1995) 4075.
[11] Ohkawa, T., Comments on Plasma Phys. Contr. Fusion **12** (1989) 165.
[12] Bruma, C., Cuperman, S., Komoshvili, K., J. Plasma Phys. **57** (1997) 805.
[13] Cuperman, S., Bruma, C., Komoshvili, K., J. Plasma Phys. **56** (1996) 149.
[14] Komoshvili, K., Cuperman, S., Bruma C., J. Plasma Phys. **57** (1997) 611.

Captions to figures

Fig.1. Test of the computational algorithm used in this paper: (a) Comparison of numerical solutions for the vacuum case with the corresponding analytical ones indicated by the symbols $\Delta, \circ, +$ and $\times$; the relevant physical parameters: $\epsilon \equiv R/a = 1/10, n(0) = 10^{14}\, cm^{-3}, B_0(0) = 1\, T, n = -3$ and $m = -1$. The temperature $T = 100\, eV$. (b) Modification of 'all-vacuum' solutions in the presence of plasma: the numbers $0, \ldots, 0.5$ on the curves represent the values of the factor multiplying the actual plasma density at $r = 0$, $n(0)$. (c) Dependence of the field solutions on the density of grid points: the solid curve corresponds to 2000 grid points; the results corresponding to 10,000 grid points are marked by black squares. (d) Frequency spectrum of the total power absorption, $P(\omega)$; the dashed curve corresponds to the case $E_{||} = 0$. The frequency range is that of the Alfven continuum, $\omega \geq \omega_L$. (Wave frequencies are measured in units of the ion cyclotron frequency at $r = 0$.)

Fig.2. Frequency spectra of the total absorbed power, $P(\omega)$ (solid curves) and total current drive, $I(\omega)$ (dotted curves) for aspect ratios 10(a), 5(b), 3(c), 2(d), 1.6(e), 1.4(f), 1.3(g) and 1.1(h) and a temperature value $T = 100\, eV$; $n(0) = 10^{14}\, cm^{-3}, B_0(0) = 1\, T$.

Fig.3. As Fog.2, but for $T = 500\, eV$.

Fig.4 Inverse-aspect-ratio dependence of the maximum efficiency $\eta_{max} = \eta(\omega_L)$ for several combinations of poloidal (m) and toroidal (n) wave numbers: see keys on figures. (a) $T = 100\, eV$; (b) $T = 500\, eV$. The other parameters are the same as in Fig.1. In all cases, $\omega = \omega_L(m, n, \epsilon, T)$ — the lower edge of the Alfven continuum.

Fig.5a,b. Inverse-aspect-ratio (ϵ) and frequency (ω) dependence of the radial distance (from the axis) X_s at which the conversion from the fast magnetosonic wave to Alfven wave occurs, for several combinations of toroidal and poloidal wave numbers: (a),(g) $(m, n) = (-1, -1)$; (b),(h) (-1,-2); (c),(i) (-1,-3); (d),(j) (-2,-1); (e),(k) (-2,-2); (f),(l) (-2,-3). The temperature $T = 100\, eV$ in (a) –(f) and $T = 500\, eV$ in (g) - (l).

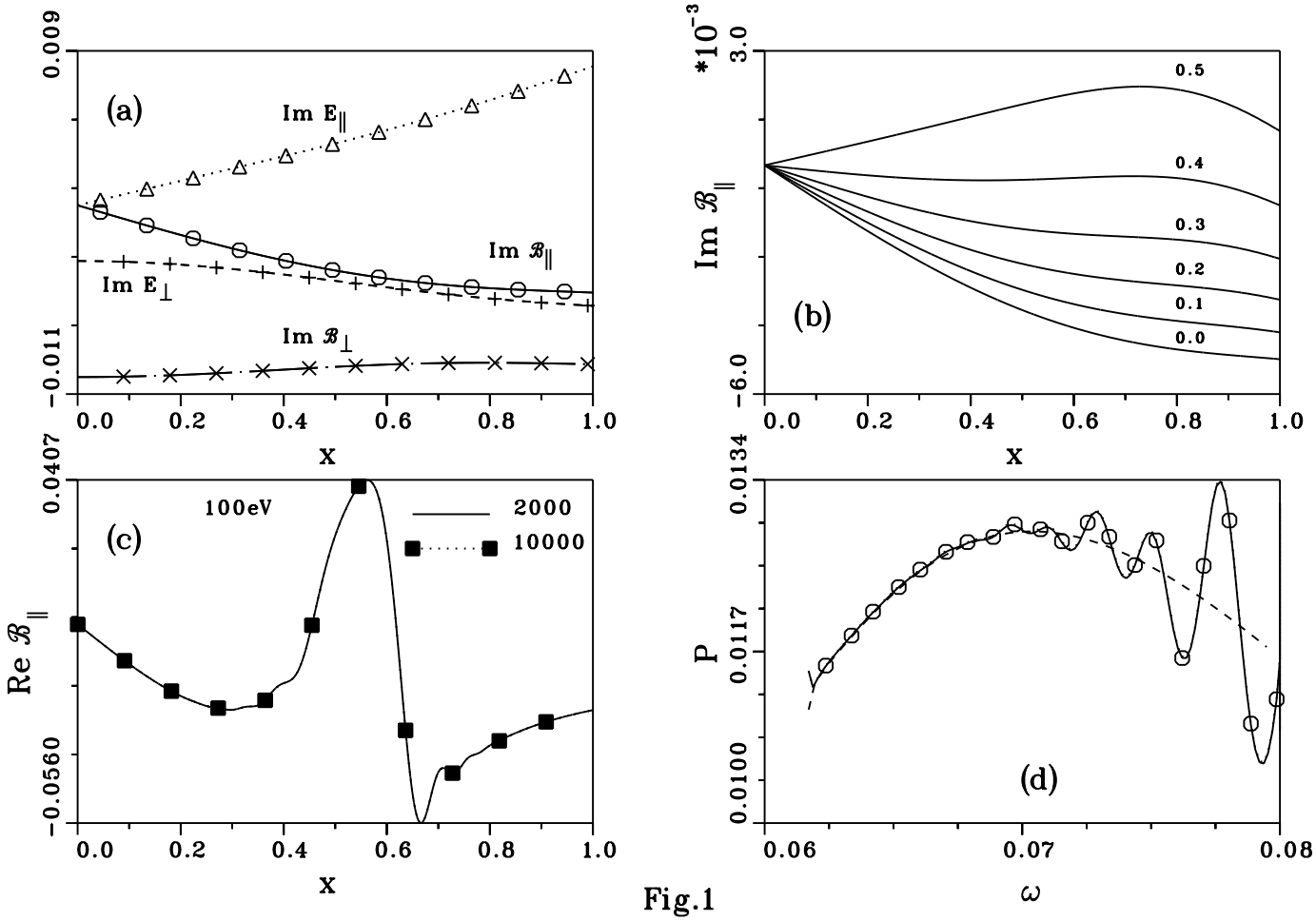
(a)
Im E∥
Im ℬ∥
Im E⊥
Im ℬ⊥
0.009
−0.011
0.0
0.2
0.4
0.6
0.8
1.0
x
(b)
*10^-3
3.0
−6.0
Im ℬ∥
0.5
0.4
0.3
0.2
0.1
0.0
(c)
100eV
2000
10000
Re ℬ∥
0.0407
−0.0560
(d)
P
0.0134
0.0117
0.0100
0.06
0.07
0.08
ω

Fig.1

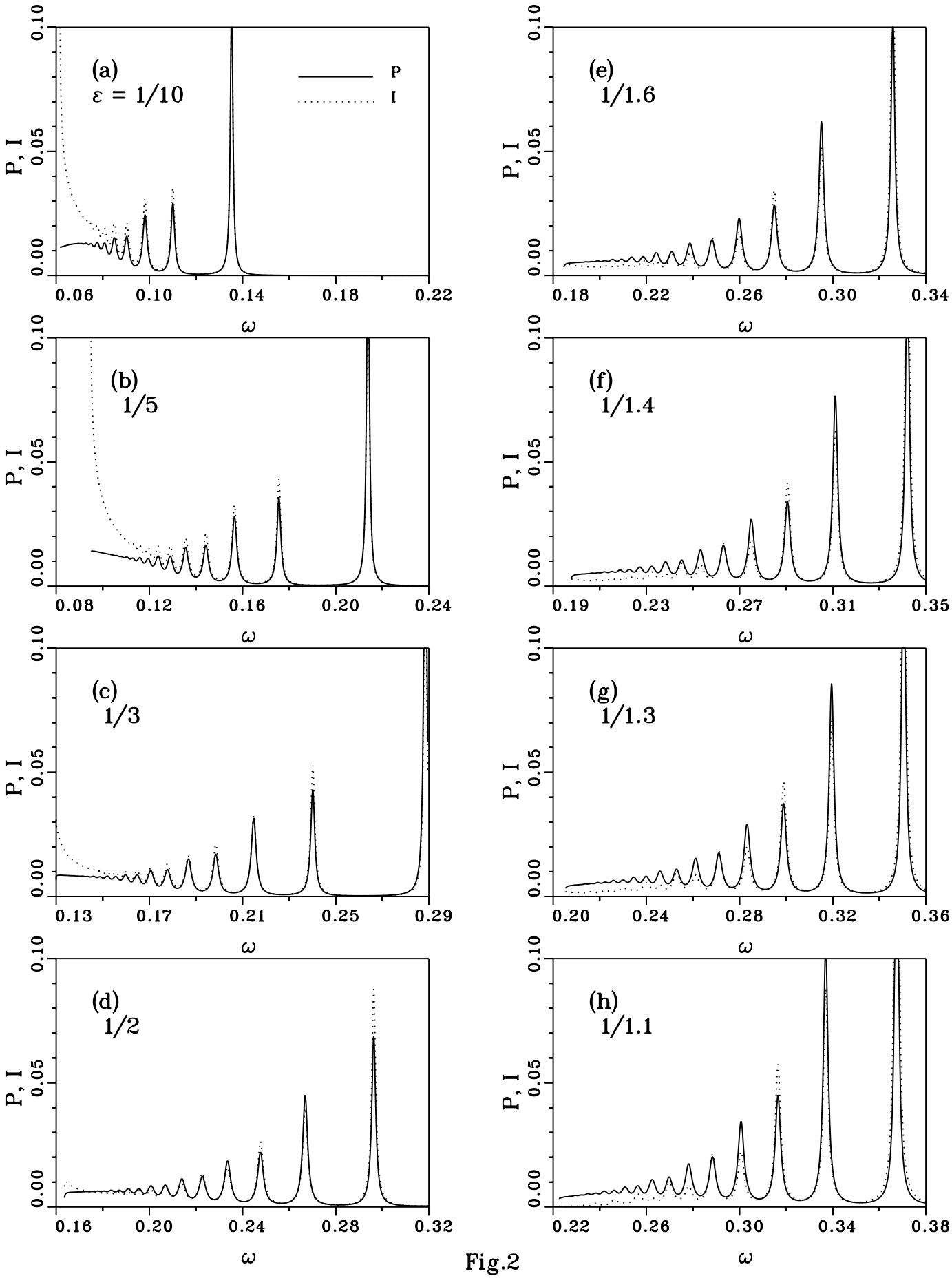

Fig.2

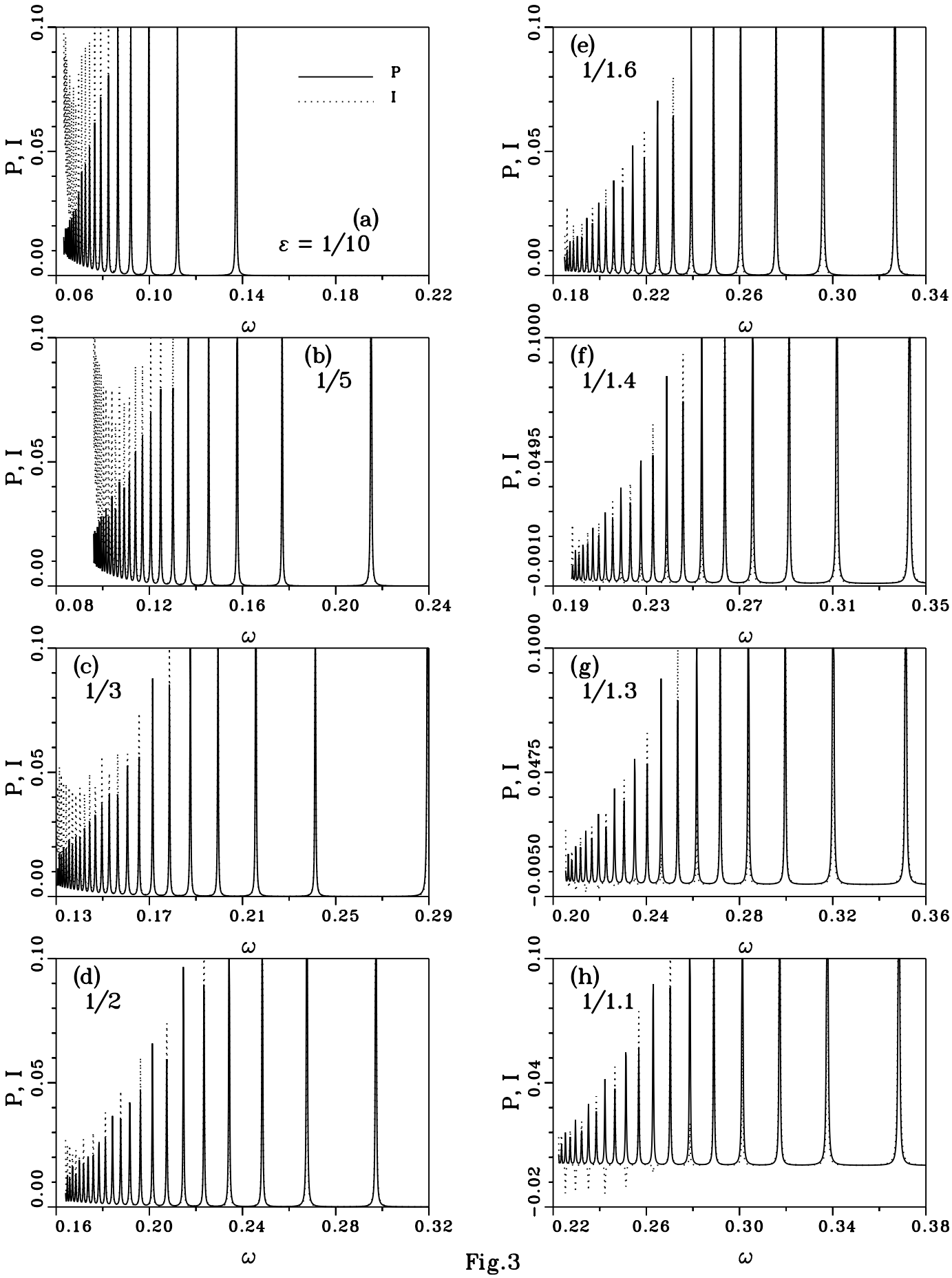

Fig.3

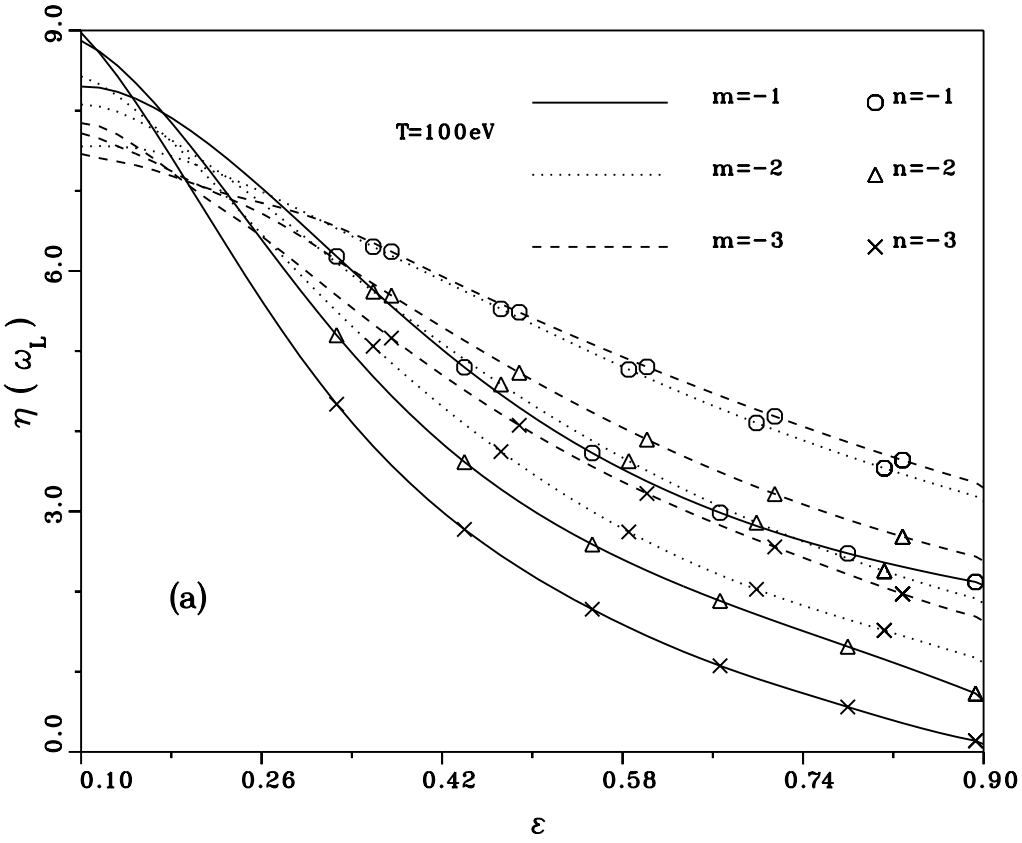
T=100eV
m=-1
m=-2
m=-3
n=-1
n=-2
n=-3
(a)
η (ω_L)
ε
0.0
3.0
6.0
9.0
0.10
0.26
0.42
0.58
0.74
0.90

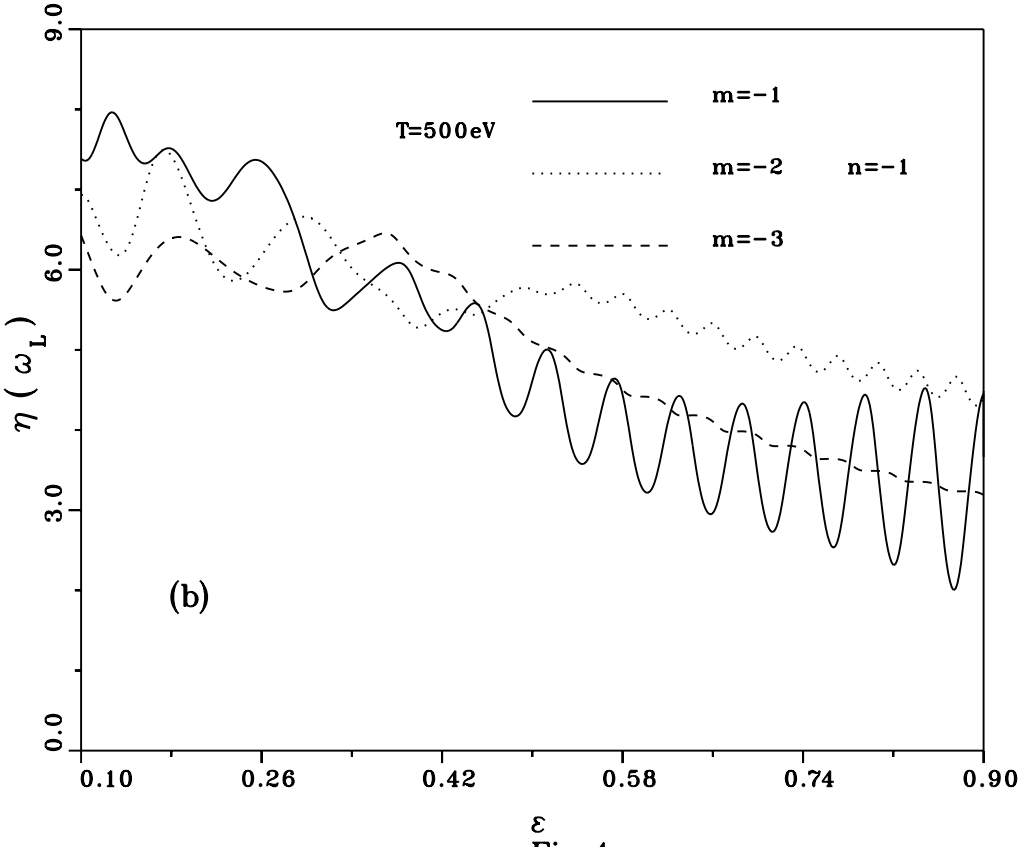
T=500eV
m=-1
m=-2
m=-3
n=-1
(b)
η (ω_L)
ε
0.0
3.0
6.0
9.0
0.10
0.26
0.42
0.58
0.74
0.90

Fig.4

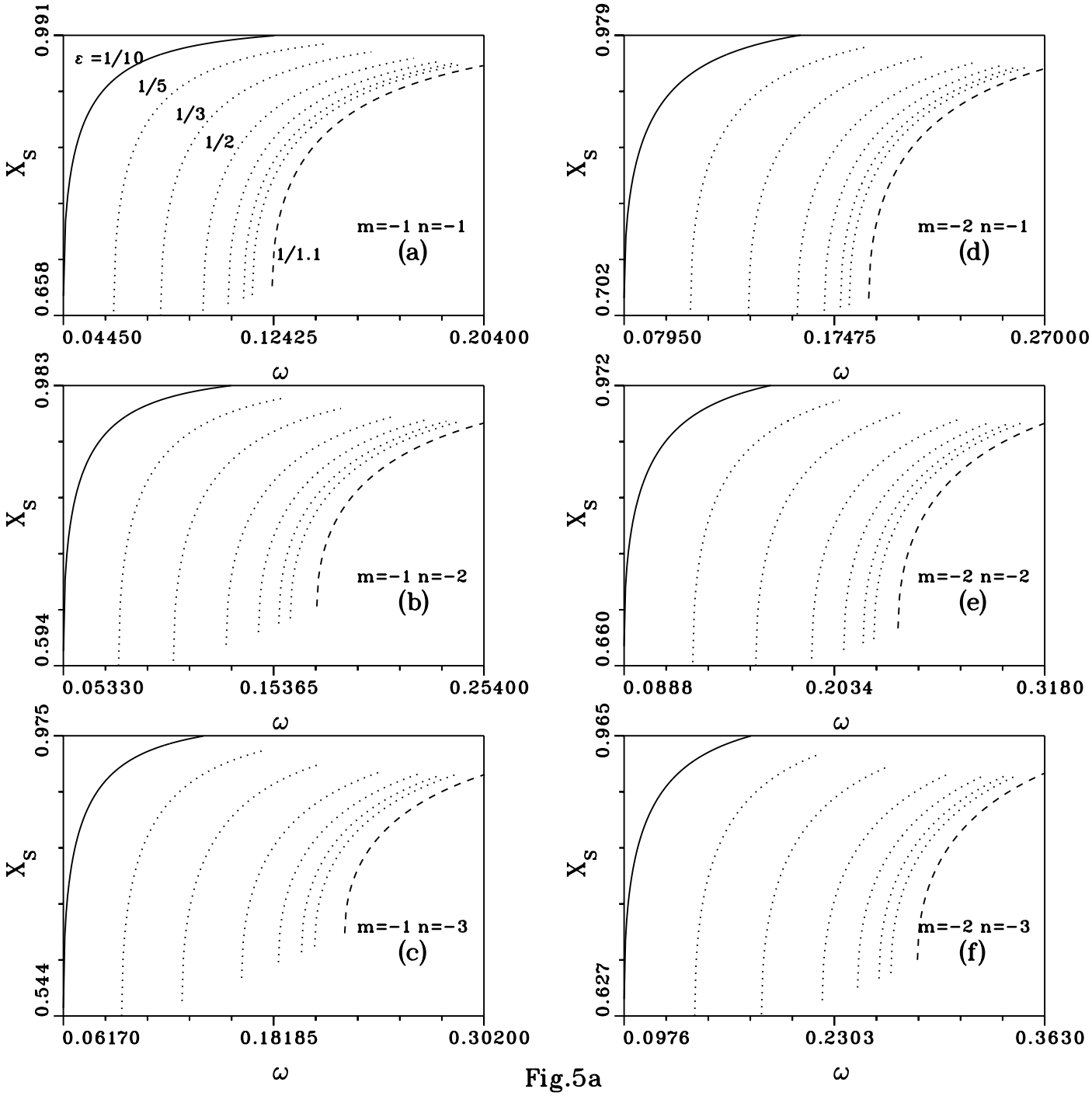
ε =1/10
1/5
1/3
1/2
1/1.1
m=−1 n=−1
(a)
m=−2 n=−1
(d)
m=−1 n=−2
(b)
m=−2 n=−2
(e)
m=−1 n=−3
(c)
m=−2 n=−3
(f)
X_S
ω
0.991
0.658
0.04450
0.12425
0.20400
0.979
0.702
0.07950
0.17475
0.27000
0.983
0.594
0.05330
0.15365
0.25400
0.972
0.660
0.0888
0.2034
0.3180
0.975
0.544
0.06170
0.18185
0.30200
0.965
0.627
0.0976
0.2303
0.3630

Fig.5a

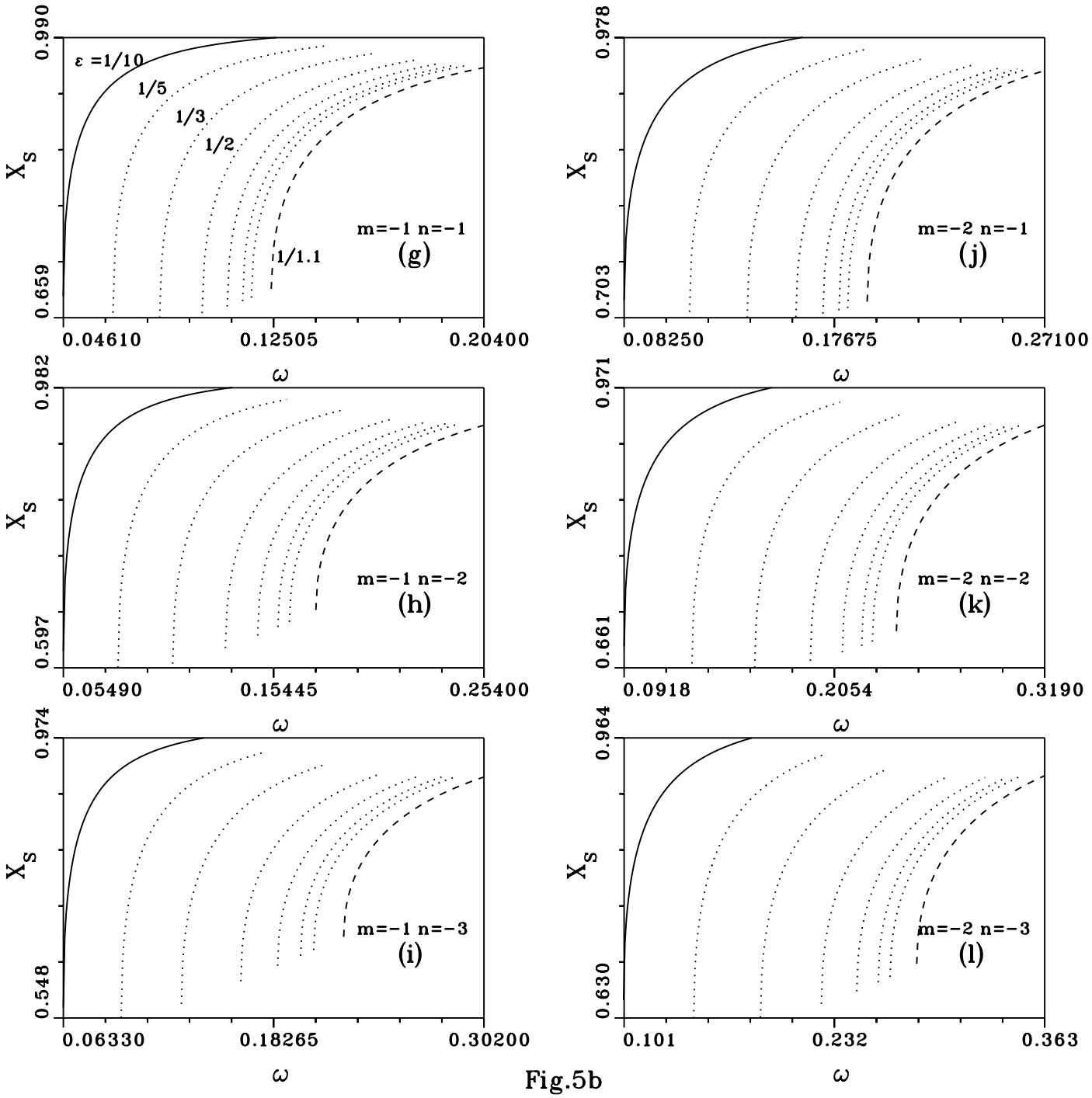
ε =1/10
1/5
1/3
1/2
1/1.1
m=−1 n=−1
(g)
m=−2 n=−1
(j)
m=−1 n=−2
(h)
m=−2 n=−2
(k)
m=−1 n=−3
(i)
m=−2 n=−3
(l)
X_S
ω
0.990
0.659
0.04610
0.12505
0.20400
0.978
0.703
0.08250
0.17675
0.27100
0.982
0.597
0.05490
0.15445
0.25400
0.971
0.661
0.0918
0.2054
0.3190
0.974
0.548
0.06330
0.18265
0.30200
0.964
0.630
0.101
0.232
0.363

Fig.5b